Tellus (2000), 52A, 330–345
Printed in UK. All rights reserved

TELLUS
ISSN 0280–6495

Thermocline ventilation and pathways of tropical–subtropical water mass exchange

By SCOTT HARPER*, *Program in Atmospheric and Oceanic Sciences, Department of Geosciences, Princeton University, USA*

(Manuscript received 14 April 1998; in final form 8 November 1999)

ABSTRACT

The mechanism of thermocline ventilation is investigated using a global, high-resolution ocean GCM, with realistic topography and surface wind forcing. Because 2-dimensional representations of circulation can be misleading, the subsurface flow is examined by visualizing the trajectories of particles which subduct in the mid-latitudes and travel within the ventilated thermocline. Three model runs are performed, each with identical surface forcing but with different initial particle distributions. Results from these runs show that the pathways of water mass exchange between the tropics and the subtropics are functions of the surface wind forcing, background density structure, and basin geometry. In the Pacific, ventilated waters from the northern and southern mid-latitudes reach the tropical thermocline through both the western boundary and the interior of the basin. In the Atlantic Ocean, the equatorial thermocline is ventilated primarily through water mass exchange with the southern hemisphere alone. In the Indian Ocean, the pathways of water mass exchange have patterns similar to those in the Atlantic and Pacific basins, though the lack of a mid-latitude gyre in the northern basin restricts the deep subduction and ventilation to the southern hemisphere.

1. Introduction

The theory of the ventilated thermocline, as presented by Luyten et al. (1983), has been developed analytically over the past fifteen years. Recently, simple numerical models have been used to take a closer look at the details involved in the subduction and subsequent flow of waters within the thermocline (McCreary and Lu, 1994; Lu and McCreary, 1995; Lu et al., 1998). However, these idealized models are often unable to resolve some aspects of the 3-dimensional interior flow, particularly when more complex surface forcing and basin geometries are prescribed. In order to apply the theory to the real ocean in a useful manner, the details of the flow, such as the pathways of water mass exchange between the tropical and extratropical thermocline, must be determined.

It appears likely that the ventilated thermocline mechanism plays a rôle in maintaining the vertical temperature structure of the equatorial ocean. Observations of tracer concentrations provide evidence of the connection between the equatorial thermocline and the mid-latitude ventilation regions, supporting results found using numerical ocean models. However, the manner in which this water mass exchange takes place is still not completely understood. Concerning the Pacific Ocean, for example, tritium observations indicate that surface waters from the mid-latitude north Pacific must be partially responsible for ventilating the thermocline in the equatorial Pacific (Fine et al., 1987). However, there has been some recent debate about the pathways through which water from the north Pacific thermocline enters the equatorial

* Corresponding address: Program in Atmospheric and Ocean Sciences, Princeton University, Princeton, NJ 08544-0710, USA.
e-mail: slharper@Princeton.EDU

undercurrent (EUC). Numerical studies of subsurface flow in the Pacific have provided contradictory results with respect to the pathways through which mid-latitude water reaches the equatorial thermocline. Some numerical studies (Lu and McCreary, 1995) suggest that the thermal structure in the north Pacific, particularly in the region of the north equatorial counter current (NECC), represents an internal barrier to subsurface flow, requiring mid-latitude thermocline water to travel to the western boundary before reaching the equator through the Mindanao current. Results from other numerical models (Liu et al., 1994 (hereafter LPP); Liu and Huang, 1998; Rothstein et al., 1998) indicate that water from the north Pacific may join the EUC through the interior ocean in the central Pacific as well as through the Mindanao current. Although this particular discrepancy arises in the Pacific, such details of thermocline ventilation are poorly known in the Atlantic and Indian Oceans as well, because asymmetric basin geometry and complex wind stress forcing complicate the simple picture described by the analytic theory.

In this paper, thermocline ventilation is studied in a high-resolution ocean GCM forced by a realistic wind stress in order to address some of the issues that simpler models have been unable to resolve. The method of analysis used here is similar to that in LPP, in which neutrally buoyant particles are placed within the ocean model domain and allowed to advect with the 3-dimensional velocity field. By examining the trajectories of the particles, a more complete picture of the interior flow can be developed. Conclusions can be drawn about the probable pathways of water mass exchange and how the mechanism of thermocline ventilation operates within this model for a given surface forcing.

The paper is organized as follows. Section 2 gives an overview of the numerical model and the applied forcing. Section 3 explains the method used for particle integration, the initial locations of the particles, and the three model runs that will be discussed. In Section 4, the results from the Pacific basin are examined, and differences between the northern and southern hemispheres are discussed. In Section 5, the notion of a dynamic "barrier" to water mass exchange near the Pacific's NECC is examined. Section 6 provides an overview of the thermocline ventilation in the Atlantic and Indian Ocean basins. The results from all three experiments are summarized in Section 7, and the potential significance of the results to various theories for decadal climate variability is considered.

2. The model

The numerical model used for this study is a version of the MOM code developed at GFDL (Pacanowski, 1996). The model domain is nearly global, spanning all longitudes and extending from 78°S to 65°N, with a single sponge layer in the north Atlantic between 55°N and 65°N. The latitudinal resolution is 1° outside the tropics, but increases to 0.33° in the region within 10° of the equator. The longitudinal resolution is 1° globally. The model contains fifty vertical levels, with 7.5 m resolution within the top 225 m, and has no explicit mixed layer parameterization at the surface.

A constant value for horizontal mixing was chosen for the model with coefficients for the eddy viscosity and diffusivity of $2 \times 10^7\,\mathrm{cm^2\,s^{-1}}$ and $1 \times 10^7\,\mathrm{cm^2\,s^{-1}}$, respectively. In the vertical, mixing is determined by a Richardson number dependent scheme (Pacanowski and Philander, 1981) with an additional small depth-dependent coefficient used as a background value (Bryan and Lewis, 1979), as the Richardson number scheme by itself tends to be too weak outside of the tropics. A sponge layer restores the temperature and salinity to Levitus (1982) climatology in the north Atlantic between 55°N and 65°N. The time constant for restoration varies linearly from 40 days at 55°N to 4 days at 65°N. At the surface, the model temperature and salinity are relaxed to Levitus monthly values with a 10 day time constant.

The initial conditions for each experiment come from the end of a 21-year spin-up run forced by monthly climatological winds (Hellerman and Rosenstein, 1983) and surface temperatures (Levitus, 1982). All three model runs were forced by this monthly-varying climatology, starting from January conditions. The only differences between each run were the number of particles followed and their initial distribution, the nature of the information recorded at each particle location, and the length of the integration.

3. Particle initialization and integration

Because the flow field within the thermocline is 3-dimensional and time varying, 2-dimensional plots of the stream function are difficult to interpret and can be misleading (Liu et al., 1994). Instead, a Lagrangian approach is used here in which trajectories, created by the advection of particles within the model's velocity field, are used to observe the model circulation. A new location for each particle is computed during each model time step and a record of these locations is maintained throughout the integration. The Lagrangian trajectories created in this manner are meant to represent the motion of water parcels within the interior ocean, and information about the pathways of water mass exchange may be inferred. However, because the particles do not necessarily carry water properties along with them, care must be taken when interpreting the results. Trajectory analysis offers certain advantages over alternative methods, such as the transport of an artificial tracer concentration, in that trajectories can reveal water mass transport over broad, shallow pathways which can be difficult to distinguish when looking at the depth-integrated concentrations of passive tracers alone.

For the model runs discussed here, the trajectories are created as follows. At the beginning of the run, each particle is given an initial latitude, longitude, and depth. At every time step, the local velocity of each particle is computed from a 3-dimensional linear interpolation of the velocity at the nearest eight grid points. Using this velocity, a new particle position is calculated using a simple forward-time-step integration. The particle position is constrained to the model domain, so that if the new location places the particle within land (which may happen near a lateral boundary for example), it is moved to the nearest location that still lies within the model's velocity field. Every 10 days of model time, the current positions are written to file so that the trajectory of each particle can be examined after the run is complete. Errors in the trajectories can arise from the discretization of the velocity term, though it is difficult to estimate how much the final pathways might be affected. These errors are dependent on both the spatial and temporal resolution of the model, as well as the nature of the local velocity field around each particle (Haidvogel, 1982). The high vertical and horizontal resolution used for these integrations will keep the relative error of the final trajectories within reasonable limits. In addition, most of the flow within the thermocline is much less turbulent than the surface flow, increasing the credibility of those trajectories that travel within the ventilated thermocline. Also, because the particle integration is done using the instantaneous model velocities at each 2-h time step, errors that would arise from using monthly or weekly averages are avoided.

Three model runs will be discussed, each of which had a different initial particle distribution. For the first experiment, a total of 14,400 particles were distributed globally at a depth of ten meters at the beginning of the run in January, using a uniform horizontal distribution. After four years of model time, the new locations of the particles were examined to determine the regions where the most sinking, or "subduction", had taken place. Fig. 1 shows the positions of the particles after 4 years, with the color of the particle representing its final depth. From this plot it is evident that, as expected, the majority of the subduction in this simulation occurs in the mid-latitudes, between the tropical easterlies and the subtropical westerlies. It is in this region that the curl of the climatological wind stress reaches its maximum strength, shown in Fig. 2. This strong wind curl results in downward Ekman pumping which, along with lateral induction and seasonal changes in thermocline depth, is responsible for the subduction of water from the mixed layer into the main thermocline (Huang and Qiu, 1994).

The initial particle positions for the second experiment were chosen with the information from the first experiment in mind. In the 2nd model run, a total of 10,000 particles were initially placed at a depth of 10 m in five specific mid-latitude subduction regions. Fig. 3 shows the location of these 5 regions, chosen towards the eastern side of the basins to allow comparison with the results from LPP. The number of particles and their horizontal distribution vary between the five regions, but this will not affect the intercomparisons between the basins presented here. 3000 particles were placed in both the north Pacific and north Atlantic, 2000 in the southern Pacific, and 1000 each in the southern Atlantic and Indian Oceans. The model was integrated for 40 years, allowing the particles to subduct from the surface

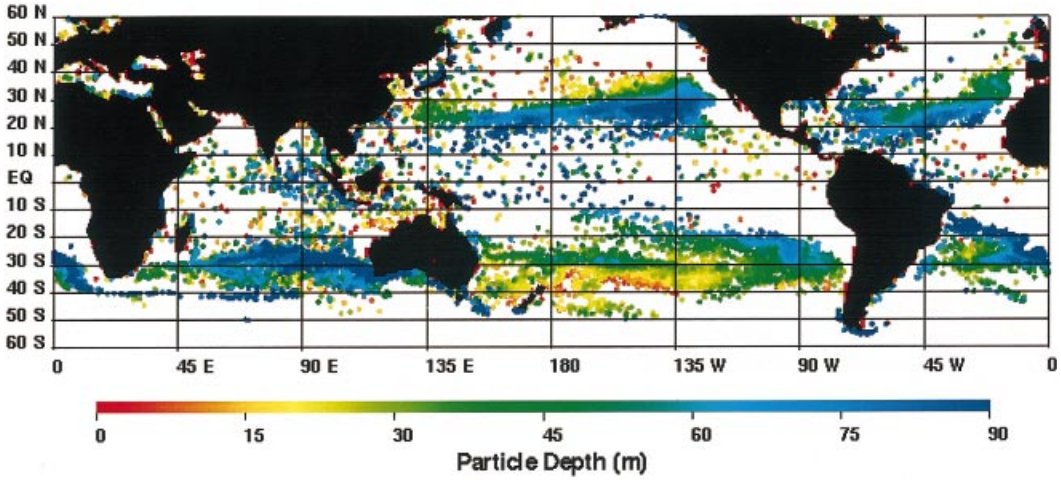

Fig. 1. Position and depth of 14,400 particles after four years of model integration. The particles were initially released at a depth of ten meters with a globally uniform spacing in the horizontal. Color represents the depth attained through Ekman pumping after 4 years.

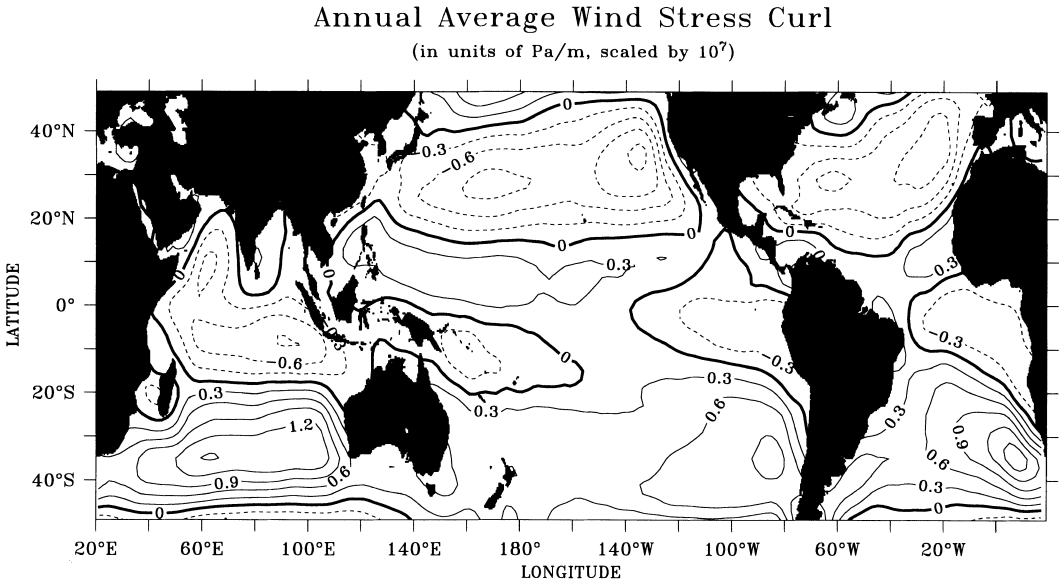

Fig. 2. Annual average wind stress curl of the winds used for surface forcing.

levels into the main thermocline and either ventilate the equatorial ocean or recirculate within the subtropical gyres.

In a 3rd experiment, the particle trajectory code was updated so that the local ocean conditions at each particle location could be recorded along with the position at ten day intervals. The quantities calculated were local temperature, salinity, relative vorticity, planetary vorticity, and density. These values were found using the same linear interpolation used to compute the particle velocity. By plotting these values along individual trajectories, the conservative nature of each quantity within the model can be examined. For this 3rd experi-

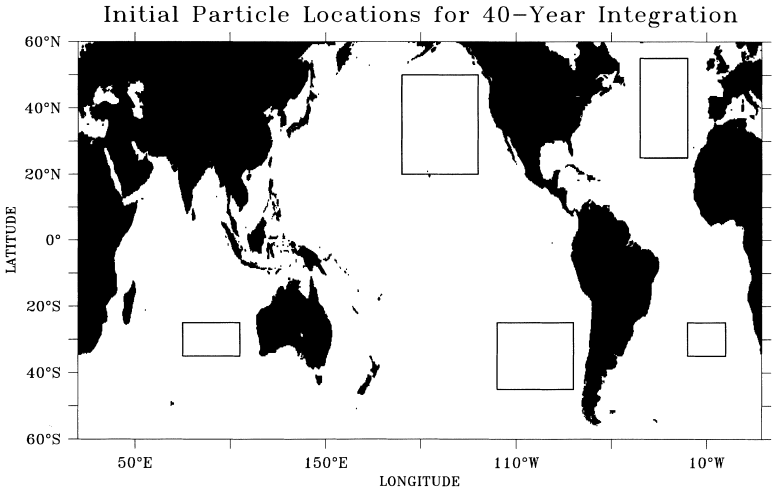

Fig. 3. The 5 regions chosen as the initial locations for the 10,000 particles released at the start of the second experiment.

ment, 2430 particles were followed for a period of 20 years. The initial particle locations for this run were chosen to address some particular issues concerning the pathways of water mass exchange and the dynamics of thermocline ventilation.

4. Results from the Pacific

Results shown in Fig. 1 indicate that, for this simulation, the surface subduction in the mid-latitudes of the north Pacific is stronger than the subduction in the south Pacific. This result is in accord with the stronger wind stress curl in the north Pacific. The subduction region in the South, however, is larger and extends farther to the east due to the asymmetric basin geometry about the equator. This will have an impact on the exchange pathways found in the second experiment. It should be noted that analyzing the Lagrangian motion of a specific set of particles, while very useful for some applications, is limited in that source information can only be obtained for the location and time the particles are released. In these experiments, the particles are initially placed in the surface level during January. Therefore, the thermocline ventilation associated with Ekman pumping is observed, but not the ventilation due to lateral induction into the thermocline, such as that which occurs in the subsurface in the Kuroshio region (Huang and Qiu, 1994). The actual timing of the particle initialization is not critical in these experiments because there is no downward momentum arising from convective adjustment. Therefore, although it is primarily the water from the late winter mixed layer that is pumped into the main thermocline, the neutral particles subduct slowly over a period of a few years, with the mixed layer water properties of the sesonal thermocline changing around them until they reach the permanent thermocline.

A cursory glance at a sub-sample of the particle trajectories from the second experiment, shown in Fig. 4, reveals that in this simulation there are significant differences between the northern and southern hemispheres concerning the pathways of water mass exchange with the equatorial Pacific. This is expected, as asymmetries in the basin geometry, wind forcing, and mean current structure about the equator should lead to different characteristics of water mass exchange from the north and the south. The basic geometry of the Pacific basin can explain some of the differences, in that the trajectories of particles from the south are more likely to reach the equator because the subduction region in the south Pacific extends about 50° farther eastward than the one in the north Pacific. Because the average equatorward velocity of the particles within the thermocline is similar in both hemispheres, particles that subduct

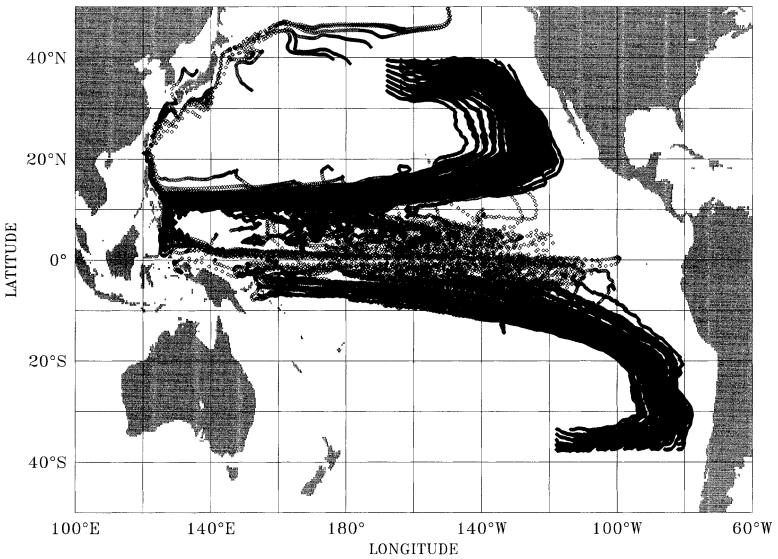

Fig. 4. A sub-sample of particle trajectories in the Pacific Ocean, shown after 20 years of model integration. Markers represent particle locations at 10-day intervals. The differences between the exchange pathways from the northern and southern hemispheres are evident.

farther to the east have more time to reach the equator before arriving at the western boundary. Thus, for a given westward zonal velocity, particles that subduct in the narrower north Pacific are more likely to arrive at the western boundary before reaching the equatorial ocean by a direct route.

However, another more significant asymmetry between the North and south Pacific lies in the mean surface wind forcing. The ITCZ, located north of the equator between 5°N and 12°N, drives an Ekman upwelling circulation in the upper ocean that induces an eastward geostrophic current across the Pacific. This current, the north Equatorial counter current (NECC), and the dynamic height field associated with it have a significant effect on the pathways of particles from the north. 5 sample trajectories from the 3rd experiment are shown in Fig. 5. The trajectories denoted "A" and "B" represent the pathways traveled by 2 particles during the first 10 years of model integration. The two particles were initially placed at a depth of ten meters and positioned at latitudes 20° from the equator towards the eastern side of the Pacific basin. The particles subducted in the mid-latitudes and followed the subtropical gyres equatorward and westward. Their pathways are similar until the particle from the north (A) reaches the latitude of the NECC. Here, the particle's zonal velocity, which is primarily geostrophic, changes from westward to eastward due to the influence of the dynamic height field associated with the ITCZ. The northern particle then travels to the southeast until reaching the southern extent of the NECC around 5°N, at which point its zonal velocity reverses again. It then follows a southwestern trajectory until being entrained by the EUC at the equator. During the journey, the meridional velocity of the particle is almost always equatorward with a nearly constant magnitude. The meridional velocity for the particle originating in the southern hemisphere is also steady and of similar magnitude. Fig. 6 shows the local latitude, density and total potential vorticity of the two particles plotted against time during their travel along the interior pathway to the equator. They will be discussed further in Section 5.

Despite the differences exhibited by particles A and B in Fig. 5, there are many basic similarities between trajectories flowing within the ventilated thermocline in each hemisphere. After subducting at the eastern edge of either the northern or southern sub-tropical gyres, a particle will typically do one of three things: recirculate within the

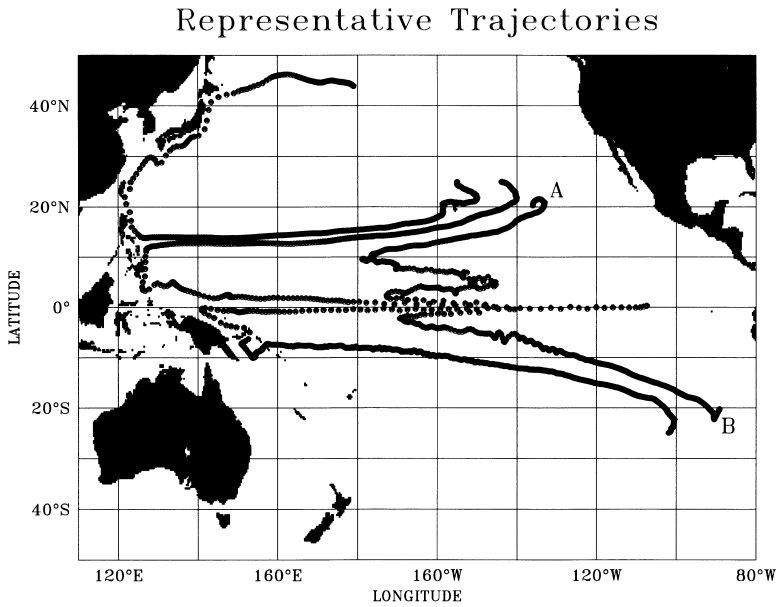

Fig. 5. Representative trajectories from the Pacific Ocean. In the north Pacific, the recirculating window, western boundary exchange window, and interior exchange window. Only the two exchange windows are shown from the southern hemisphere. The A and B trajectories show the differing pathways of interior exchange from the northern and southern hemisphere.

gyre after turning poleward at the western boundary, join the EUC in the western tropical Pacific after turning equatorward at the western boundary, or join the EUC in the Pacific interior without reaching the western boundary. These three pathways are represented by the trajectories shown in the upper half of Fig. 5. In LPP, the source regions of the three different pathways could be determined by the longitude at which the particles originally subducted, like "windows" between the subduction regions at the ocean's surface and various destinations within the ventilated thermocline. Particles that follow the gyre to the western boundary and then turn poleward must subduct through the "recirculating window". Particles that turn equatorward upon reaching the western boundary must enter the thermocline through the "western boundary exchange window" eastward of the recirculating window. Finally, particles from the mid-latitudes that reach the equator through the interior ocean must subduct even farther eastward in the "interior exchange window". (The upper half of Fig. 5 can be compared with Fig. 8a in LPP.)

The limits of each window along an outcropping isopycnal could be easily determined in LPP because of the simplified constant wind stress used to force their model. The windows in this simulation, forced by a more complex time-dependant wind stress, are less obvious, though a rough estimate for each window can be determined for a specific subducting latitude. If we choose a latitude of 30°N in the north Pacific, the recirculating window lies westward of 155°W and the interior exchange window lies eastward of 140°W, with the western boundary exchange window situated between the two. At 30°S in the south Pacific, the recirculating window lies to the west of 110°W, the western boundary exchange window outcrops between 110°W and 95°W, and the interior exchange window lies eastward of 95°W. Of course, the trajectories of the particles that enter through the interior exchange window in the north Pacific are obviously different from those found by the model in LPP, because the wind stress used in the LPP simulation did not generate a north equatorial counter current. The "bifurcation point" at the western boundary of the north Pacific (dividing the impinging NEC between the northward Kuroshio and the southward Mindanao

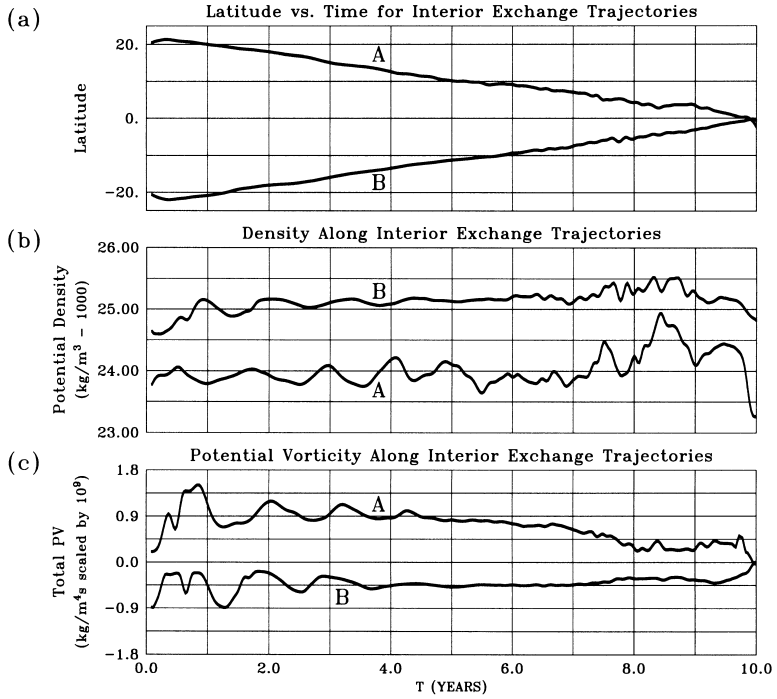

Fig. 6. (a) Latitude of the particles A and B shown in Fig. 4 during their 10-year journey to the equatorial Pacific. (b) Potential density at the particle locations along each trajectory. (c) Total potential vorticity at the particle locations along each trajectory.

currents) occurs near 13°N in this simulation. This is the same latitude found by Toole et al. (1990) using observations from hydrographic surveys. This latitude is also similar to the bifurcation point in the LPP simulation, although the idealized wind stress used to drive that model constrained the location of the bifurcation latitude to 12°N.

For studies of climate variability, it can be useful to obtain a measure of the advective timescale involved in ventilating the equatorial thermocline. Using the trajectories, we can get an estimate for the average travel time between the mid-latitude subduction region and the equator by recording the time when each particle reaches the EUC. The histograms in Fig. 7a, b show the range of travel times for particles released at the surface in the mid-latitudes to reach the equatorial ocean through the ventilated thermocline. Only particles with an initial latitude from 25° to 45° from the equator were used so a direct comparison between the hemispheres could be made. The average travel time is about 2 decades for the particles from the north Pacific, with a peak time of 21 years. On average, it takes longer for the particles from the southern hemisphere to reach the equator, and the peak time around which most particles arrive is not as pronounced. This advective time scale is of importance to proposed mechanisms for climate variability which use the ventilated thermocline to advect mid-latitude temperature anomalies into the tropics, such as the one presented in Gu and Philander (1997). Although the time scales found in this study are for neutral particles, an investigation into the advection time required for an active tracer, such as a temperature anomaly, to ventilate the equatorial thermocline is being performed.

It is also possible to estimate the advection time required for particles to recirculate within the mid-latitude gyres. Fig. 7c shows a histogram of the time taken for particles released in the north Pacific to return to the release region by way of the Kuroshio after travelling to the western bound-

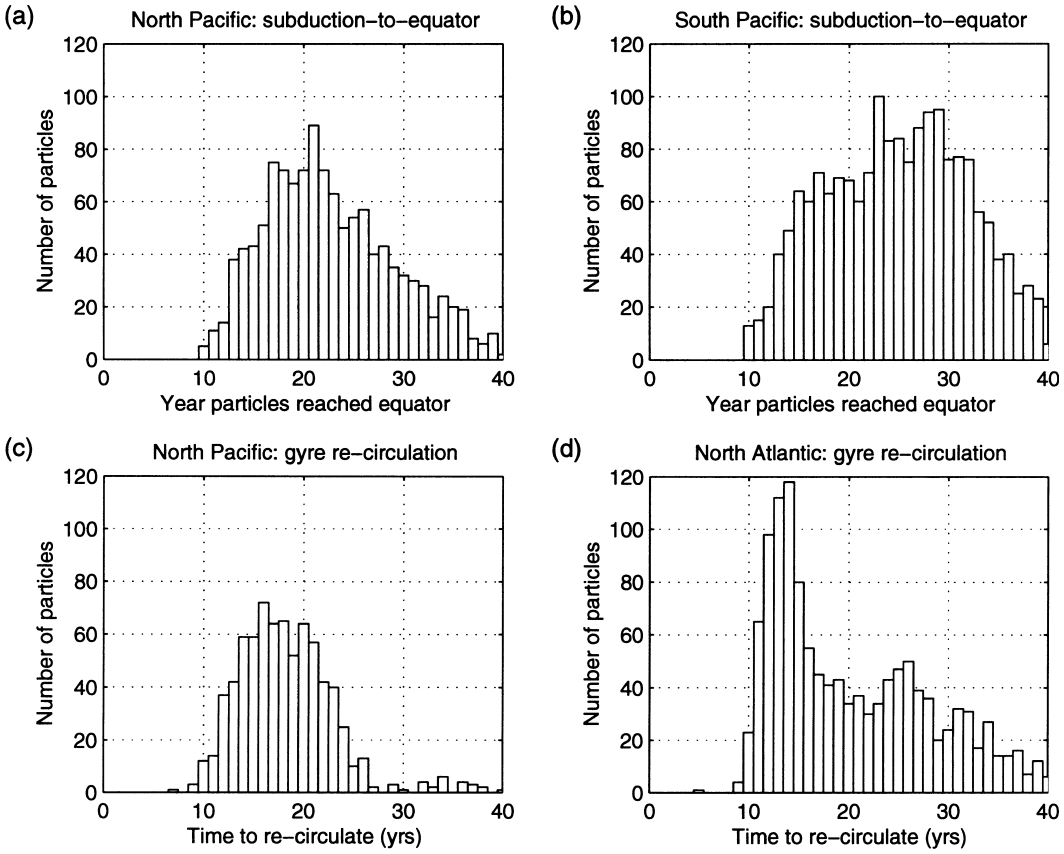

Fig. 7. (a) A histogram of the time required for particles from the north Pacific to reach the equator from the mid-latitude subduction region. Only particles subducting between 25°N and 45°N were considered. (b) Same, but for particles from the south Pacific. (c) Times required for particles in the north Pacific to subduct, reach the western boundary, and recirculate back into the mid-latitudes into the eastern north Pacific through the thermocline. (d) Same as (c) but for the north Atlantic.

ary through the ventilated thermocline. The figure shows an average recirculation time of 16–18 years, which could be relevant to some proposed mechanisms for mid-latitude climate variability (Latif and Barnett, 1994). Further discussion of this point is presented in Section 7.

5. A barrier to internal flow?

In this simulation, as was shown in the previous section, there are particles from the north Pacific that reach the EUC through the interior ocean. In doing so, they pass through the region of the NECC which, as suggested by Lu and McCreary (1995, hereafter LM), might act as a "barrier" to southward interior flow in the real ocean. They concluded, based on results from a 2.5 layer model of the Pacific driven by realistic winds, that the presence of the ITCZ created a region of high potential vorticity that blocked the interior exchange of water between the equator and the subtropical north Pacific. LM point out that because the flow within the thermocline is basically geostrophic, in the absence of large horizontal velocity gradients the flow should conserve potential vorticity in the simplified form of f/h (where f represents the Coriolis parameter and h represents the thickness of an isopycnal layer). Under the ITCZ, Ekman upwelling brings denser water

towards the surface, forcing a compression of the isopycnals in that region. This larger density gradient (or smaller h) between 5°N and 12°N results in a higher potential vorticity under the ITCZ when compared with waters to the north or south. Hence, if a parcel of water is physically constrained to conserve potential vorticity, it will not be able to move southward over this potential vorticity (PV) barrier, and can only reach the equator through a western boundary current. Therefore, since f decreases equatorward in the northern hemisphere, the argument by LM is that for f/h to be conserved, h must monotonically decrease equatorward as well. Because it does not (due to the ITCZ), a water parcel which conserves potential vorticity cannot cross the region of the NECC.

This argument seems valid when considering a meridional cross section of the thermal structure, but does not hold for the 3-dimensional circulation. The critical factor is that north of the NECC, the water is not only moving southward towards the equator, but westward as well. If a cross section at 155°W, such as the one observed by Wyrtki and Kilonsky (1984), were representative of the entire Pacific, then a complete barrier might exist. Instead, the potential vorticity on most isopycnal surfaces in the tropics tends to be lower in the west due to the lower stratification. Fig. 8 shows the total potential vorticity at 10°N plotted against density. The lower PV in the western basin allows water masses that wouldn't be able to cross the PV barrier directly at a particular longitude to travel to the southwest until reaching a region in which there is no PV gradient to the south. Fig. 9 shows the PV on the 24.0 sigma-level isopycnal, computed from the model's climatology. This plot shows features similar to those found in Talley (1988), where the Levitus (1982) observed data was used to compute and map PV on isopycnal surfaces. Ventilated waters, following the natural PV contours on an isopycnal, will turn to the southeast in the region under the ITCZ and continue travelling towards the equator.

We can use the trajectories created during the 3rd experiment to examine this phenomenon. Going back to Fig. 6, the three plots show the latitude, density and total potential vorticity for particles A and B in Fig. 5 during their journey along the interior exchange pathway. Fig. 6a can be used to determine when particle A passes through the NECC, moving across the proposed PV barrier sometime after the fifth year. At this

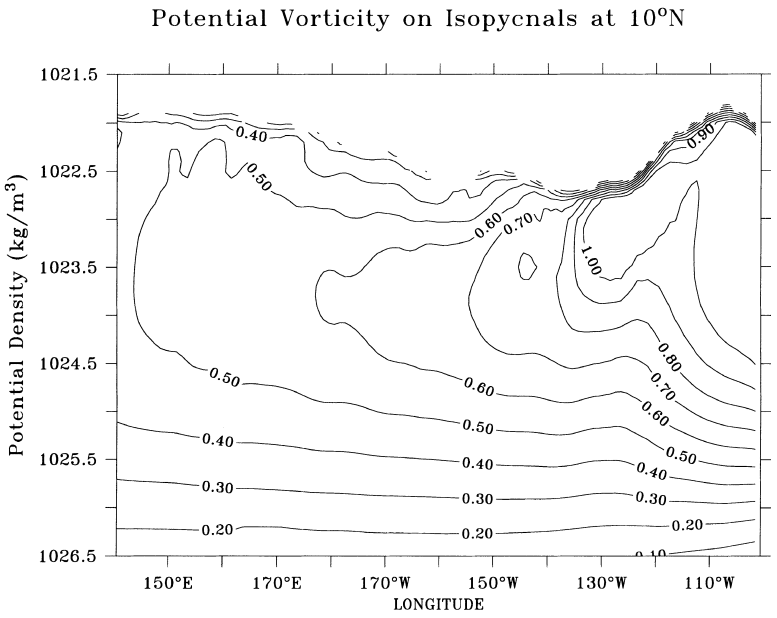

Fig. 8. A cross section of total potential vorticity on isopycnal surfaces in the Pacific at 10°N. Values of potential vorticity are lower in the western basin, allowing water masses to cross the potential vorticity "barrier".

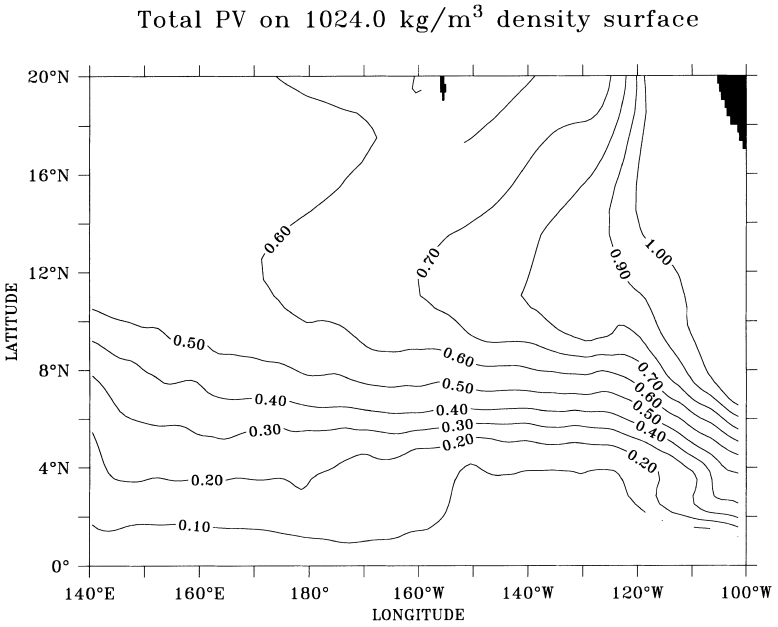

Fig. 9. A map of the total PV on the 24.0 sigma-level in the model. Water masses can follow PV contours until mixing and relative vorticity balances dominate near the equator.

time, there are no corresponding jumps in the PV or the density, as the particle has simply traveled to the southwest following the contours of PV on that isopycnal until it reaches a point at which it may flow to the southeast. Thus, the thermal structure under the ITCZ in this simulation merely redirects the pathways of thermocline ventilation, rather than creating a true PV barrier in the interior ocean.

The argument against a complete barrier from the north is also supported by observational data of tracer concentrations. Fine et al. (1987) discuss the existence of a tritium maximum in measurements taken along the equator in the central Pacific, with a maximum in tritium concentration near 140°W. This feature can be observed in the particle data from this simulation as well by recording the longitude at which each particle first reaches the EUC. This data can be binned to show the primary longitudes at which the particles flow onto the equator. A histogram is provided in Fig. 10a that shows the longitudes at which particles released in the north Pacific reach the equatorial Pacific. The peak west of 150°E represents particles from the western boundary exchange window, where the particles join the EUC through the Mindanao current. When arriving eastward of 160°E, the particles represent the interior pathway of water mass exchange. Of the particles that reach the equator through the interior, there is a peak in the number from the north Pacific between 160°W and 150°W, similar to the position of the observed tritium maximum. The depth of the particles that reach the equator through the interior is also similar to the depth of the tritium maximum, as most particles from the north Pacific join the EUC between 130–170 m at that longitude. (Particles originating at the surface in the southern mid-latitudes reach the equator a little deeper, primarily between 150–200 m.) McPhaden and Fine (1988) give a dynamical interpretation for the tritium maximum, suggesting that there is a meridional geostrophic flow from the north onto the equator in that region of the central Pacific. This idea has been further refined by Liu and Huang (1998), who show that the vertical structure of the geostrophic flow is of importance for determining the source region. The results presented in Fig. 10a indicate that it could indeed be the arrival of north Pacific water through the interior that leads to the tritium maximum in the central equatorial Pacific.

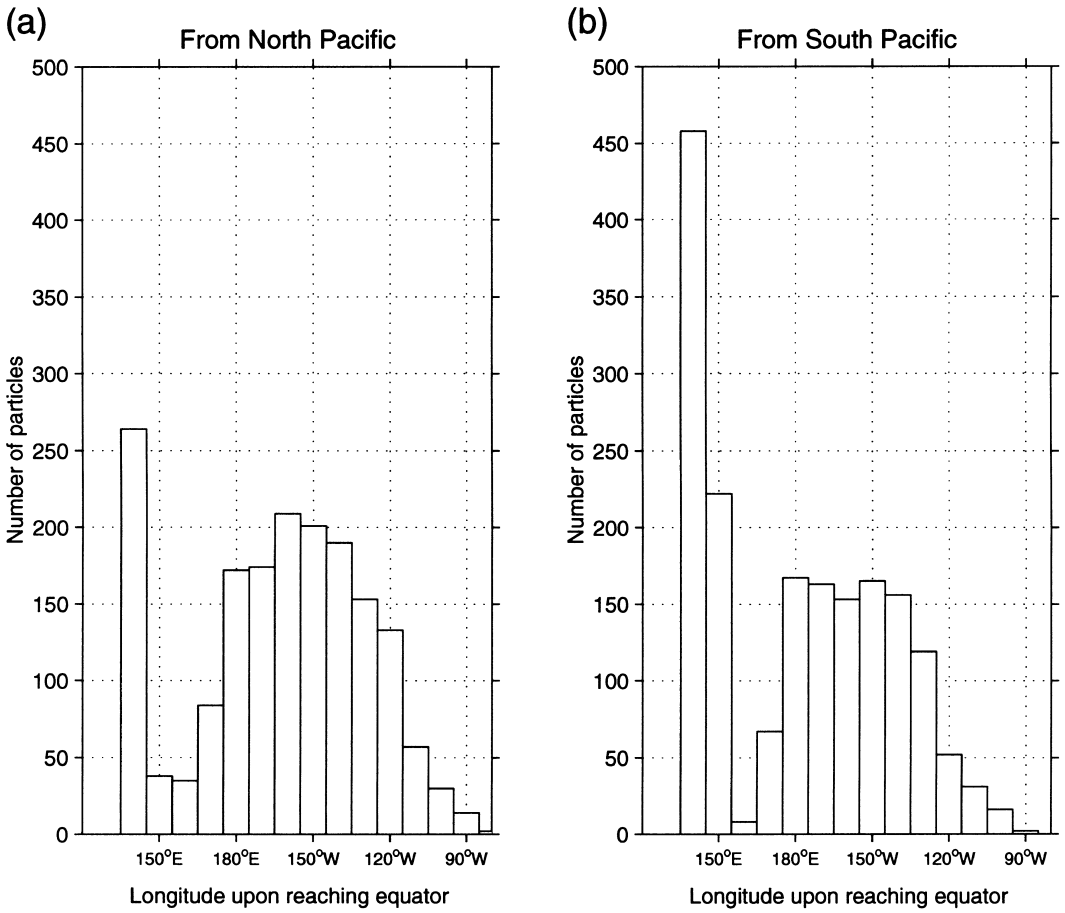

Fig. 10. Histograms of the longitudes at which subducted particles reach the equator. (a) From the North Pacific, there is a peak in the number of particles arriving in the central Pacific near 150°W. Only about 1/4 of the particles enter the EUC by way of the western boundary (apparent as the maximum at 140°E). (b) From the South Pacific, about 1/2 of the particles that reach the equator travel through the western boundary.

It is also apparent from the histogram in Fig. 10a that of the north Pacific particles that reached the equator, more than 3/4 did so through the interior ocean rather than through the western boundary. Again, the Lagrangian particles examined here can only represent the thermocline waters created through Ekman pumping, so although more particles from the north Pacific reach the equator through the interior, it is not clear if, overall, more water from the north Pacific is exchanged with the equatorial ocean through the Mindanao current in the western basin. Fig. 10b shows a similar histogram for the particles originating the south Pacific, where there is a more equal distribution between the number of particles which take the interior pathway and the number that reach the equator by way of the western boundary.

In their paper, LM acknowledge that the results from their model cannot explain this maximum, but suggest that tropical instability waves may be responsible for transporting water to the EUC. However, the discrepancy may actually result from the lower resolution in the LM model, as suggested by Liu and Huang (1998) and Lu et al. (1998). In any case, the particle trajectory data presented here, along with the observational tracer data, do not indicate that there is a total barrier to water

mass exchange through the interior of the north Pacific.

6. Equatorial thermocline ventilation in other basins

6.1. Atlantic Ocean

Particle trajectories from the Atlantic show that in this simulation the equatorial thermocline is primarily ventilated by water from the southern hemisphere, at least with respect to the subduction arising from Ekman pumping. This is predominantly a result of the basin geometry in the north Atlantic. Fig. 11 shows a subsample of Atlantic trajectories from the second experiment after 15 years. In the North, particles that subduct on the far eastern side of the subtropical gyre are blocked from travelling southward by the northwestern coast of Africa. These particles rise from the thermocline back into the upper levels of the model, creating a "shadow zone" that extends to the southwest off the coast of Africa, as predicted by theory (Luyten et al., 1983). The eastern-most particles that are not blocked remain within the ventilated thermocline and reach the western boundary of South America at a latitude of 12°N. However, unlike those in the Pacific, particles in the north Atlantic do not turn equatorward in this simulation, as the Guyana Current flows to the northwest along the Brazilian coast. Because of this, over 95% of the particles subducted into the thermocline through the surface in the north Atlantic flow into the Caribbean and recirculate back to the north Atlantic through the Gulf Stream. As shown in Fig. 7d, the time scale for this recirculation peaks around 14 years.

In the South Atlantic, the mid-latitude gyre extends all the way to the equator, as it does in the south Pacific, and both the interior and western boundary exchange windows are able to ventilate the Atlantic equatorial thermocline. However, as the basin width of the southern Atlantic is much narrower than the Pacific, the interior exchange window is smaller, and the primary pathway of water mass exchange is through the western boundary. The bifurcation point at the western boundary in the South Atlantic occurs at a latitude of 18°S in this simulation. Particles arriving southward of 18°S recirculate within the subtropical gyre while particles that reach the western boundary equatorward of that latitude flow northward beneath the Brazil current, joining the Atlantic EUC upon reaching the equator.

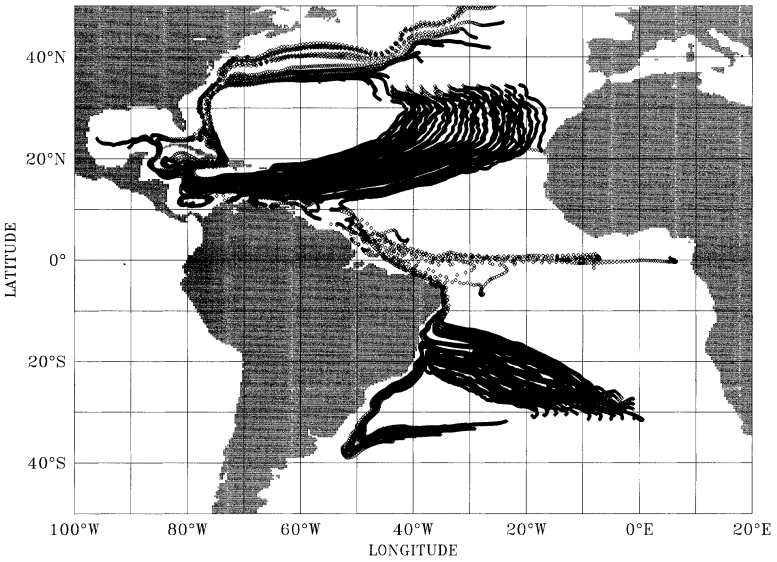

Fig. 11. A sample of ventilation trajectories in the Atlantic Ocean. It appears difficult for particles subducted through the surface in the north Atlantic to reach the equatorial Atlantic.

6.2. Indian Ocean

The Indian Ocean presents a more difficult setting in which to investigate the ventilated thermocline mechanism and tropical–extratropical water mass exchange. Among the reasons for the complexity are the absence of a subtropical gyre in the northern basin, a strong seasonal cycle in the upper ocean, the lack of an established equatorial current system similar to those in the Atlantic and Pacific, and an additional source of thermocline ventilation in the Indonesian throughflow. Fig. 1 showed that, for this wind forcing, significant subduction occurred in the southern mid-latitudes while no organized regions of sinking existed in the limited northern reaches of the Indian Ocean (the Bay of Bengal and the Arabian Sea). The particle trajectories from the second experiment, shown in Fig. 12, show that a ventilated thermocline mechanism operates in the model's southern Indian Ocean, but the fate of the subducted particles is less deterministic than in the other basins, where it was possible to define the three subduction windows. Particles sink off the western coast of Australia, reaching greater depths than in other subduction zones, and follow a path to the northwest, eventually arriving at the eastern coast of Madagascar. In this simulation, all particles turn equatorward, flowing around the northern tip of the island to reach the eastern coast of Africa near 12°S. This is the bifurcation point for the southern Indian, with 75% of these particles following trajectories towards the equator and the rest returning to the mid-latitudes with the Agulhas current. It takes the particles an average of eighteen years to reach the western boundary from the southern mid-latitudes. In contrast to the other oceans in this simulation, most of the equatorward-flowing particles do not join an undercurrent at the equator, as the Indian Ocean does not have a strong EUC. For the most part, the particles that turn to the north either spread slowly to the east at latitudes just off the equator or travel to the southeast back across the basin as shown in Fig. 12. It is apparent that the idea of exchange windows does not particularly hold in the Indian Ocean, as the disruption of the subsurface flow around Madagascar prevents the initial longitude of subduction from having any bearing on the eventual fate of the particle.

7. Summary and discussion

By examining the ventilated thermocline mechanism within the context of a high-resolution numerical model, it was hoped that some of the questions concerning pathways of water mass

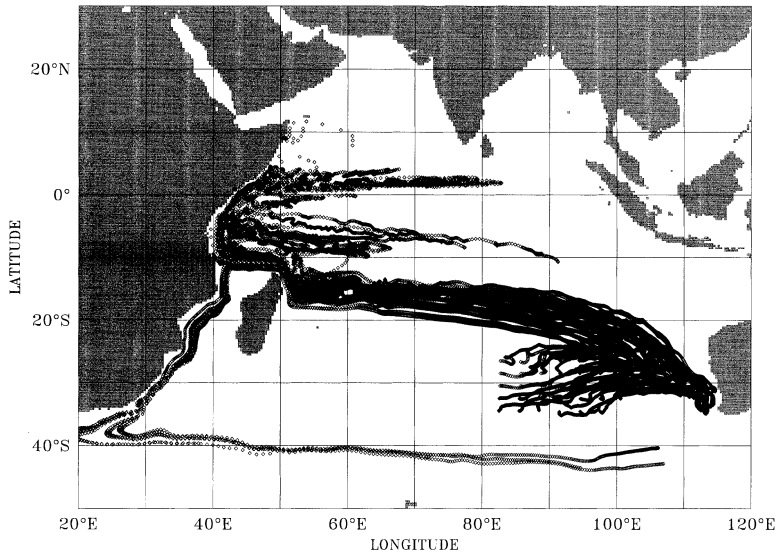

Fig. 12. A sample of ventilation trajectories in the Indian Ocean. The low-latitude ventilation differs from that in the Atlantic and Pacific because of the unique equatorial current structure of the Indian basin.

exchange could be answered. Because the flow is complex and 3-dimensional, a method of analysis employing the advection of particles was used to visualize flow in the main thermocline. In the Pacific, the equatorial thermocline is ventilated from both hemispheres in this simulation, with water mass exchange occurring through both the western boundary as well as the interior ocean. In the Atlantic, the majority of the subtropical water that ventilates the equatorial thermocline in this simulation comes from the southern hemisphere. In the Indian Ocean, there is ventilation from water subducted in the southern mid-latitudes, but the equatorial current structure is more complex than that of the Atlantic or Pacific. The source waters for equatorial Indian Ocean ventilation in this model must lie in regions not covered by the initial particle locations chosen for these simulations.

Though of great value in visualizing flow fields, it should be noted that using particle advection as an analysis tool is not equivalent to following an artificial tracer concentration, as the particles are not constrained to carry water mass properties along with them. However, the fact that quantities such as potential density are largely conserved along sub-surface trajectories indicates that these trajectories may be reasonable representations of the pathways of water masses in the model. If the trajectories are reliable indicators of the advective pathways, then the advective time scales found here may be relevant to proposed mechanisms for interdecadal climate fluctuations. For example, the mechanism for climate variability discussed by Gu and Philander (1997) would be highly dependant on the advective time scale for tropical–subtropical water mass exchange, found here to be on the order of 21 years.

With respect to the north Pacific recirculation time, the particles within the thermocline travel around the subtropical gyre in about 16–18 years in this simulation. This is similar to the interdecadal time scale found by Tourre at al. (1999) when analyzing the variability in ocean temperature and sea level pressure over the northern Pacific. Using the results from a coupled GCM, Latif and Barnett (1994) outline a mechanism for mid-latitude variability in the Pacific which has a similar 20-year time-scale in their model, though the mechanism they describe involves an unstable air-sea interaction rather than the purely advective time scale found here. However, their mechanism does involve planetary waves interacting with the mean horizontal currents, so the advective time scale found in this study may still be relevant to the dynamics of that mode.

In the north Atlantic, the recirculation time of 13–14 years is in line with the results from observational studies of SST variability (Deser and Blackmon, 1993; Sutton and Allen, 1997) and subsurface temperature variability (White and Cayan, 1998). The north Atlantic trajectories in this simulation also follow a similar route as the observed SST anomalies shown by Hansen and Bezdik (1996). Grötzner et al. (1998) describe a mechanism found in a coupled GCM for Atlantic variability that is similar to the Latif and Barnett (1994) mode in the Pacific. Their mode has an 18 year time scale, but with structure similar to the 10–15 year mode found in Sutton and Allen (1997).

If water mass properties (such as anomalous temperatures) are preserved within the ventilated thermocline, they can play a rôle in climate variability through interaction with the atmosphere many years after their initial subduction, as proposed in Gu and Philander (1997). Additionally, subsurface anomalies may also affect the sea surface temperatures along the advective pathways, altering the air-sea heat exchange and providing and interdecadal scale "memory" for a coupled mode, as in the Latif and Barnett (1994) mechanism. The potential for such feedbacks to exist requires further study to determine if anomalies in water mass properties within the thermocline can be maintained over long periods of time, and if the magnitudes of such anomalies are large enough to have a discernible impact on the coupled ocean–atmosphere system.

8. Acknowledgements

The author is indebted to A. Rosati and M. Harrison for their assistance with the numerical model, along with G. Philander, D. Gu, Z. Liu and P. Chang for many helpful discussions. The calculations were carried out on a Cray T90 at the GFDL/NOAA. This research was supported by grants from the National Oceanic and Atmospheric Administration (NA56GP0226) and the Jet Propulsion Laboratory (JPL-960900).

REFERENCES

Bryan, K. and Lewis, L. J. 1979. A water mass model of the world ocean. *J. Geophys. Res.* **84**, 2503–2517.

Deser, C. and Blackmon, M. L. 1993. Surface climate variations over the North Atlantic Ocean during winter: 1900–1989. *J. Climate* **6**, 1743–1753.

Fine, R., Peterson, W. H. and Ostlund, H. G. 1987. The penetration of tritium into the tropical Pacific. *J. Phys. Oceanogr.* **17**, 553–564.

Grötzner, A., Latif, M. and Barnett, T. P. 1998. A decadal climate cycle in the North Atlantic ocean as simulated by the ECHO coupled GCM. *J. Climate* **11**, 831–847.

Gu, D. and Philander, S. G. H. 1997. Interdecadal climate fluctuations that depend on exchanges between the tropics and extratropics. *Science* **275**, 805–807.

Haidvogel, D. B. 1982. On the feasibility of particle tracking in Eulerian ocean models. *Ocean Modelling* **45**, 4–9.

Hansen, D. V. and Bezdek, H. F. 1996. On the nature of decadal anomalies in North Atlantic sea surface temperature. *J. Geophys. Res.* **101**, C4, 8749–8758.

Hellerman, S. and Rosenstein, M. 1983. Normal monthly mean wind stress over the World Ocean with error estimates. *J. Phys. Oceanogr.* **13**, 1093–1104.

Huang, R. X. and Qiu, B. 1994. Three-dimensional structure of the wind-driven circulation in the subtropical North Pacific. *J. Phys. Oceanogr.* **24**, 1608–1622.

Latif, M. and Barnett, T. P. 1994. Causes of decadal climate variability over the North Pacific and North America. *Science* **266**, 634–637.

Levitus, S. 1982. *Climatological atlas of the world ocean.* NOAA Prof. paper 13, US Department of Commerce, Washington, DC, 173 pp.

Liu, Z., Philander, S. G. H. and Pacanowski, R. 1994. A GCM study of tropical–subtropical upper-ocean water exchange. *J. Phys. Oceanogr.* **24**, 2606–2623.

Liu, Z. and Huang, B. 1998. Why is there a tritium maximum in the central equatorial Pacific thermocline?. *J. Phys. Oceanogr.* **28**, 1527–1533.

Lu, P. and McCreary, J. 1995. Influence of the ITCZ on the flow of thermocline water from the subtropical to the equatorial Pacific Ocean. *J. Phys. Oceanogr.* **25**, 3076–3088.

Lu, P., McCreary, J. and Klinger, B. 1998. Meridional circulation cells and the source waters of the Pacific equatorial undercurrent. *J. Phys. Oceanogr.* **28**, 62–84.

Luyten, J. R., Pedlosky, J. and Stommel, H. 1983. The ventilated thermocline. *J. Phys. Oceanogr.* **13**, 292–309.

McCreary, J. and Lu, P. 1994. Interaction between the subtropical and the tropical equatorial ocean circulations: the subtropical cell. *J. Phys. Oceanogr.* **24**, 466–497.

McPhaden, M. J. and Fine, R. 1988. A dynamical interpretation of the tritium maximum in the central equatorial Pacific. *J. Phys. Oceanogr.* **18**, 1454–1457.

Pacanowski, R. C. (ed.) 1996. *"MOM 2 Version 2. Documentation, User's guide and reference manual"*. GFDL Ocean Technical report no. 3.2. Geophysical Fluid Dynamics Laboratory/NOAA, Princeton, NJ 08542.

Pacanowski, R. C. and Philander, S. G. H. 1981. Parameterization of vertical mixing in numerical models of the tropical ocean. *J. Phys. Oceanogr.* **11**, 1442–1451.

Rothstein, L. M., Zhang, R-H., Busalacchi, A. J. and Chen, D. 1998. A numerical simulation of the mean water pathways in the subtropical and tropical Pacific Ocean. *J. Phys. Oceanogr.* **28**, 322–343.

Selten, F. M., Haarsma, R. J. and Opsteegh, J. D. 1999. On the mechanism of North Atlantic decadal Variability. *J. Climate* **12**, 1956–1973.

Sutton, R. T. and Allen, M. R. 1997. Decadal predictability of North Atlantic sea surface temperature and climate. *Nature* **388**, 563–567.

Talley, L. D. 1988. Potential vorticity distribution in the North Pacific. *J. Phys. Oceanogr.* **18**, 89–106.

Toole, J.M., Millard, R. C., Wang, Z. and Pu, S. 1990. Observations of the Pacific north equatorial current bifurcation at the Philippine coast. *J. Phys. Oceanogr.* **20**, 307–318.

Tourre, Y. M., Kushnir, Y. and White, W. B. 1999. Evolution of interdecadal variability in sea-level pressure, sea surface temperature, and upper-ocean temperature over the Pacific Ocean. *J. Phys. Oceanogr.* **29**, 1528–1541.

White, W. B. and Cayan, D. R. 1998. Quasi-periodicity and global symmetries in interdecadal upper ocean temperature variability. *J. Geophys. Res.* **103**, C10, 21335–21354.

Wyrtki, K. and Kilonsky, B. 1984. Mean water mass and current structure during the Hawaii-to-Tahiti shuttle experiment. *J. Phys. Oceanogr.* **14**, 242–254.